Nanoscale Res Lett (2008) 3:205–212
DOI 10.1007/s11671-008-9138-0

NANO EXPRESS

Effect of Substrate Morphology on Growth and Field Emission Properties of Carbon Nanotube Films

Sanjay K. Srivastava · V. D. Vankar · Vikram Kumar · V. N. Singh

Received: 13 March 2008 / Accepted: 3 June 2008 / Published online: 13 June 2008

Abstract Carbon nanotube (CNT) films were grown by microwave plasma-enhanced chemical vapor deposition process on four types of Si substrates: (i) mirror polished, (ii) catalyst patterned, (iii) mechanically polished having pits of varying size and shape, and (iv) electrochemically etched. Iron thin film was used as catalytic material and acetylene and ammonia as the precursors. Morphological and structural characteristics of the films were investigated by scanning and transmission electron microscopes, respectively. CNT films of different morphology such as vertically aligned, randomly oriented flowers, or honeycomb like, depending on the morphology of the Si substrates, were obtained. CNTs had sharp tip and bamboo-like internal structure irrespective of growth morphology of the films. Comparative field emission measurements showed that patterned CNT films and that with randomly oriented morphology had superior emission characteristics with threshold field as low as $\sim$2.0 V/μm. The defective (bamboo-structure) structures of CNTs have been suggested for the enhanced emission performance of randomly oriented nanotube samples.

Keywords Carbon nanotubes (CNTs) · Bamboo-structured CNTs (BS-CNTs) · Chemical vapor deposition (CVD) · Transmission electron microscopy (TEM) · Field emission

S. K. Srivastava · V. D. Vankar · V. N. Singh
Department of Physics, Thin Film Laboratory, Indian Institute of Technology Delhi, Hauz Khas, New Delhi 110016, India

Present Address:
S. K. Srivastava (✉) · V. Kumar
National Physical Laboratory, Dr. K.S. Krishnan Marg, Pusa, New Delhi 110012, India
e-mail: srivassk@mail.nplindia.ernet.in

Introduction

Carbon nanotubes (CNTs) [1] have attracted wide attention both in the research and industrial communities because of their unique structural and physical properties. In particular, field electron emission from CNTs has been proposed to be one of the most promising as far as its practical application is concerned. This is because CNTs present many advantages over conventional Spindt (Mo, Si, etc.) emitters [2] such as (i) high chemical stability (resistance to oxidation or other chemical species) and high mechanical strength (Young's modulus $\sim$1 TPa), (ii) high melting point ($\sim$3550 °C) and reasonable conductivity (resistivity $\sim 10^{-7}$ Ωm), (iii) high aspect ratio (>1000) with very small tip radius to greatly enhance the local electric field, and (iv) easy and low cost production, longer life time and capability of producing high-current densities at low operating voltages [3].

The potential of CNTs for field emission (FE) was first reported in 1995. FE from an isolated single multiwalled CNT (MWNT) was first observed by Rinzler et al. [4] and that from a MWNT film was reported by de Heer et al. [5]. Since then a number of experimental studies on FE of MWNTs synthesized by different processes, including arc discharge and various versions of chemical vapor deposition (CVD) both with and without plasma, have been investigated [6–17]. Several parameters such as density, length of CNTs, open/closed tips, defects, adsorbates, presence of metal particles, etc., have been reported to affect the FE characteristics of MWNT films deposited catalytically by different CVD techniques [18]. However, a comparative measurement on FE properties of MWNT films of different morphology grown by a single CVD process is rarely reported. The FE properties of single-walled CNTs (SWNTs) have also been investigated

[19, 20]. Synthesis of SWNTs is, however, a high-temperature process and sometimes requires additional post-synthesis processing for FE measurements. On the other hand, controlled and low-temperature growth of CNT films is desirable for FE-based applications. CNTs grown at low temperature by any CVD process, with or without plasma, in general, have many structural defects. For example, CNTs prepared by plasma-enhanced CVD process using combination of hydrocarbon and NH_3 or N_2 have generally bamboo-structure popularly known as bamboo-shaped CNTs (BS-CNTs) [21–23] rather than pure conventional MWNTs. Therefore, structural characteristics of the MWNTs and overall morphology of the films are critical for FE. This is also important because both structure and morphology of CNT films strongly depend on growth techniques and related parameters such as temperature, catalyst, feed gases, etc. Substrate morphology may also have significant impact on the growth of CNT films, particularly in high-frequency plasma CVD process. Microwave plasma-enhanced CVD (MPECVD) is such a process and has been successfully used to deposit a variety of nanostructured carbon films ranging from diamond [24], carbon nanosheets [25] CNTs [20, 23], and carbon nanobells [26, 27] to monochiral MWNTs [28] on Si substrates. This technique offers the advantage of growing these materials at relatively lower substrate temperatures and at a faster rate. Microwave plasma operating at low pressure is a low-temperature plasma due to the non-equilibrium state between the electrons and other heavy particles in the plasma space and full of active species. The plasma not only ionizes the gas but also causes local surface heating [29]. Consequently, growth temperature could be significantly decreased compared to non-plasma CVD process. Hence the motivation of the present study was to investigate the effect of substrate morphology on the growth of CNT films by an MPECVD process and investigate their comparative FE properties and structure–morphology dependence.

In this article, CNT films with unique morphological features were deposited on substrates with different surface morphology by the MPECVD process and their FE characteristics were investigated. The correlation between structure, morphology, and FE properties of CNTs has been discussed.

Experimental

CNT films were deposited by tubular MPECVD process. The detail of the experimental set-up is described elsewhere [25]. In brief, tubular MPECVD system is equipped with a 1.2 kW 2.45 GHz microwave source and a traverse rectangular waveguide to couple the microwave to a tubular quartz tube for generating the plasma. Substrate was placed on a quartz holder that was fully electrically insulated and the substrate was immersed in the plasma zone. It is important to mention that no additional heater was used for substrate heating and no biasing was applied to the substrate. Four set of samples were deposited on p-Si (100) substrates with different initial surface morphology: (i) mirror-polished Si substrates (sample 1), (ii) mirror polished but Fe patterned (sample 2), (iii) mechanically polished having randomly distributed pits of different shape and size (sample 3), and (iv) electrochemically etched Si having uniformly distributed pores (sample 4). The mechanical polishing of Si wafer was carried out using diamond paste containing diamond particles of size ~ 1 μm for 1 h. Porous Si substrates were prepared by the electrochemical anodization of the Si-wafer. The electrochemical bath consisted of 48% hydrofluoric acid + 99% dimethyl formamide in the ratio of 1:5. A graphite sheet and Si wafer were used as cathode and anode, respectively. Aluminum (Al) thin films were deposited on the Si substrates by thermal evaporation of Al wires (LEICO Industries, New York, USA; diameter: 0.5 mm and purity 99.99%), followed by vacuum annealing at 350 °C for making proper electrical contacts. Distance between the cathode and anode was kept as 2 cm and the current density was maintained at ~ 10 mA/cm^2. The etching was carried out for 10 min. Thin films of Fe of thickness ~ 10 nm were deposited on such Si substrates by thermal evaporation of Fe ingots (CERAC Inc., USA, purity 99.95%) at a base pressure of 2.0×10^{-6} Torr. Fe patterns (20×20 μm) were made by standard photolithography lift-off technique. The Fe-coated substrates were then loaded into the MPECVD reactor for growth process. The detail of the growth process is described in our previous article [30]. The Fe-coated substrates were pretreated in NH_3 plasma for 10 min at an input microwave power of 500 W, operating pressure of 5 Torr, and NH_3 flow rate of 40 sccm. For growth, C_2H_2 was introduced at a flow rate of 20 sccm keeping other parameters constant. Under these conditions, substrate temperature was estimated to be ~ 600 °C. All the films were deposited for 10 min. After growth, plasma was switched off and samples were cooled down to room temperature under flowing NH_3 gas.

Scanning electron microscope (SEM) (LEO 435 VP) operating at 15 kV was used for surface morphological features of the substrate and films. Structural analysis of CNTs was carried out by transmission electron microscope (TEM) (Philips, CM 12) operating at 100 kV as well as FEI, Technai G20-stwin, 200 kV equipped with energy dispersive X-ray spectroscopy (EDAX) (EDAX company, USA). TEM specimen preparation is described in our previous article [23]. Field emission measurements were carried out by planar diode assembly at a base pressure of $\sim 2.0 \times 10^{-6}$ Torr. Spacing between electrodes was kept as ~ 300 μm. The FE current was measured with

increasing voltage. Emission current density was calculated by dividing the emission current with the exposed area of the sample. Emission performances of all of the four samples were analyzed using Fowler–Nordheim (F-N) model [31]. For recording FE patterns, tin oxide (TO) coated glass was set as anode and Cu-doped cadmium sulfide (CdS) films deposited by spray pyrolysis was used as anode.

Results and Discussion

SEM micrographs of mechanically polished and the electrochemically etched Si wafers are shown in Fig. 1a, b, respectively. Randomly oriented pits of different shapes and size are observed after mechanical polishing. Electrochemical etching of Si wafers produced uniformly distributed pores of size $\sim$1 μm. Figure 1c, d shows typical surface morphology of as-deposited and patterned Fe films, respectively, on mirror-polished Si wafers. The film appears to be smooth and continuous. However, continuous film after NH_3 plasma treatment resulted into semi-spherical nanoparticles of different size as shown in Fig. 1e. Average size of the nanoparticles was estimated to be $\sim$65 nm. In case of mechanically polished or electrochemically etched Si wafers, Fe nanoparticles were also found in the pits/pores after plasma treatment of Fe film on such substrates. These particles probably seeded the nucleation and growth of CNTs.

Surface morphology of CNT films deposited on such substrates is presented in Fig. 2. Sample 1 consists of high density ($>10^9$ cm^{-2}) of vertically aligned CNTs (Fig. 2a). Sample 2 also has vertically aligned CNTs but only in Fe-patterned area (Fig. 2b). This confirms that the growth in the present process is essentially catalytic. Some CNTs in the edges of the pattern are not aligned vertically but are lean toward free area. As a result, interconnection between few CNT patterns is also observed by some of the edge nanotubes. The morphology of CNT films on mechanically polished substrates (sample 3) is very interesting as shown in Fig. 2c. CNTs around the pits are aligned such as to appear like flowers. Central part of the pits seems to be free

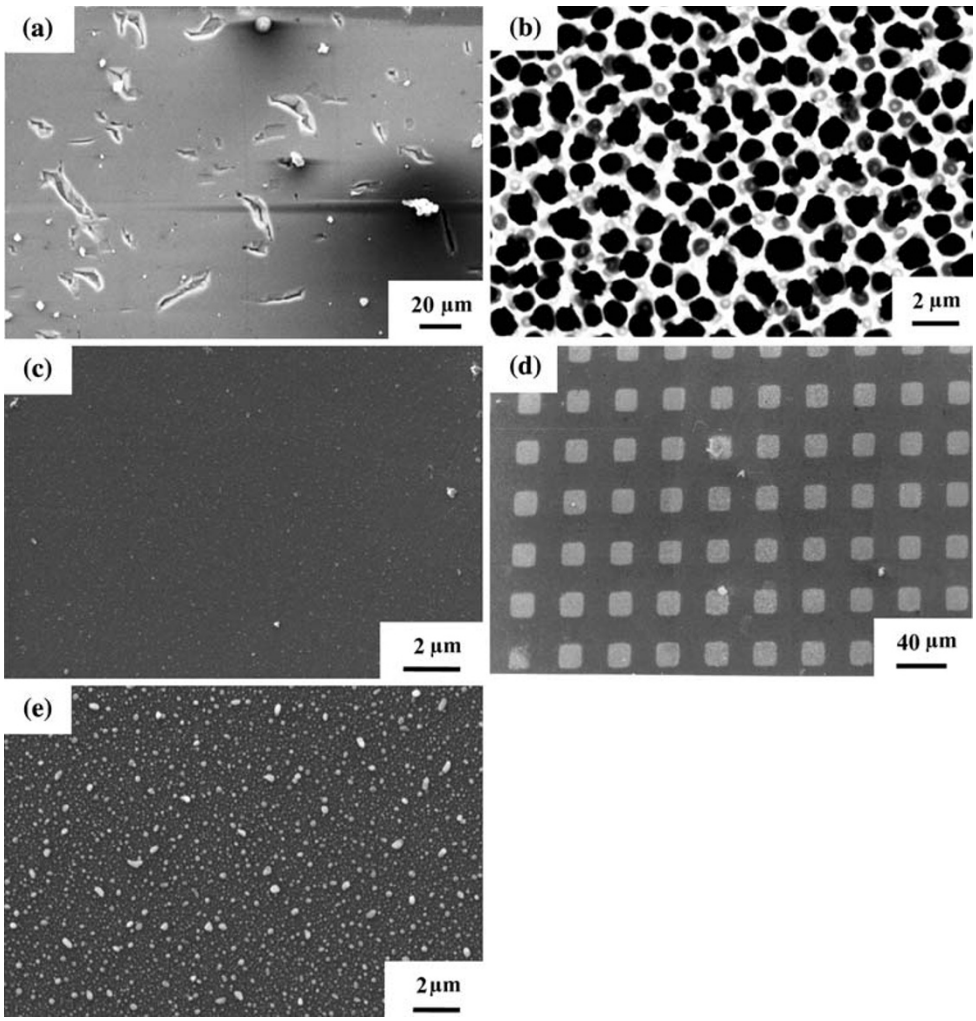

Fig. 1 SEM micrographs of (**a**) mechanically polished Si, (**b**) electrochemically etched (porous) Si, (**c**) as-deposited Fe film, (**d**) as-deposited patterned Fe film, and (**e**) NH_3 plasma-treated Fe film

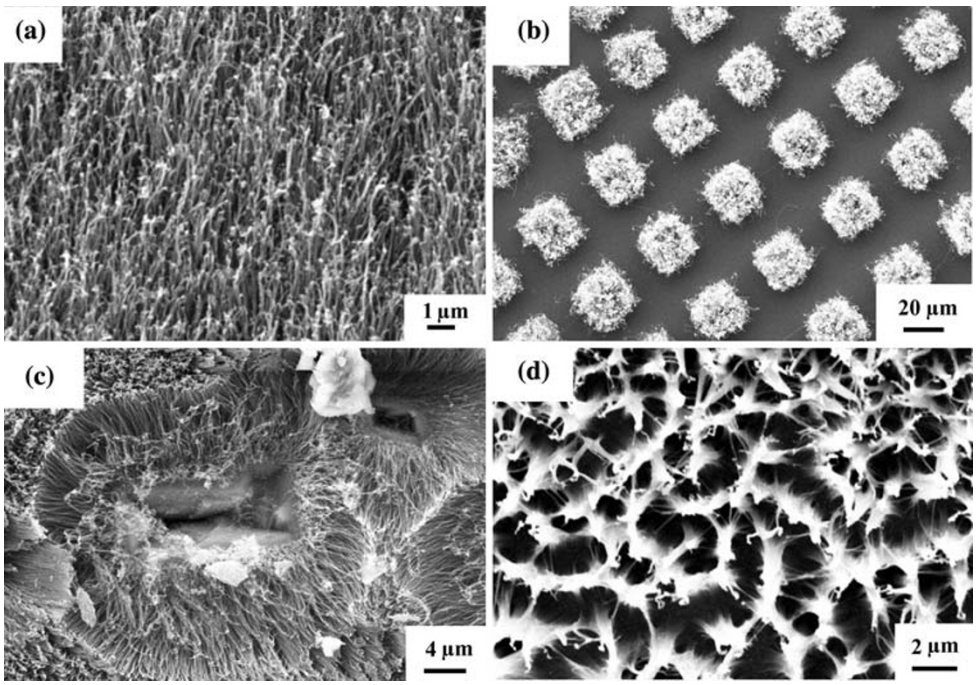

Fig. 2 SEM micrographs of CNT films: (**a**) sample 1, (**b**) sample 2, (**c**) sample 3, and (**d**) sample 4

of CNTs and nanotubes are aligned along the wall of the pits. Similar features were observed around all the pits. However, shape and size of the CNT flowers were dependent on local geometry of the pit. Figure 2d is an SEM micrograph of typical CNT films on porous Si substrates (sample 4) showing honeycomb-like morphology. Similar to sample 3, in this case also nanotubes seem to grow out from the pores along their sidewalls and finally meet together with the CNTs of nearby pores. However, for longer growth time, nanotubes merged together and the pores were not clearly visible. Average CNT length was estimated to be $\sim$20 μm in the first two samples but the length was slightly less for samples 3 and 4. The reduced length could be due to random growth orientation of CNTs.

CNTs obtained on porous/mechanically polished Si substrates have random orientations, whereas plain substrates, in general, lead to vertically aligned growth. This indicates that orientation of nanotubes is largely dependent on the local geometry of the substrate. This was further confirmed by the orientation of CNTs near the edge of the substrates. Most of the nanotubes were found to be oriented outward from the substrate edge almost normal to the side of the substrate as shown in Fig. 3. It is known that local electrostatic field gets generated on the substrate surface immersed in the plasma [32] and this may affect initial orientation of the growing nanotubes. In addition, local electric field intensity is enhanced at sharp edges in the microwave plasma [33]. It is also suggested that surface plasmon can be excited efficiently in a microwave plasma process with tubular geometry if the substrate is placed

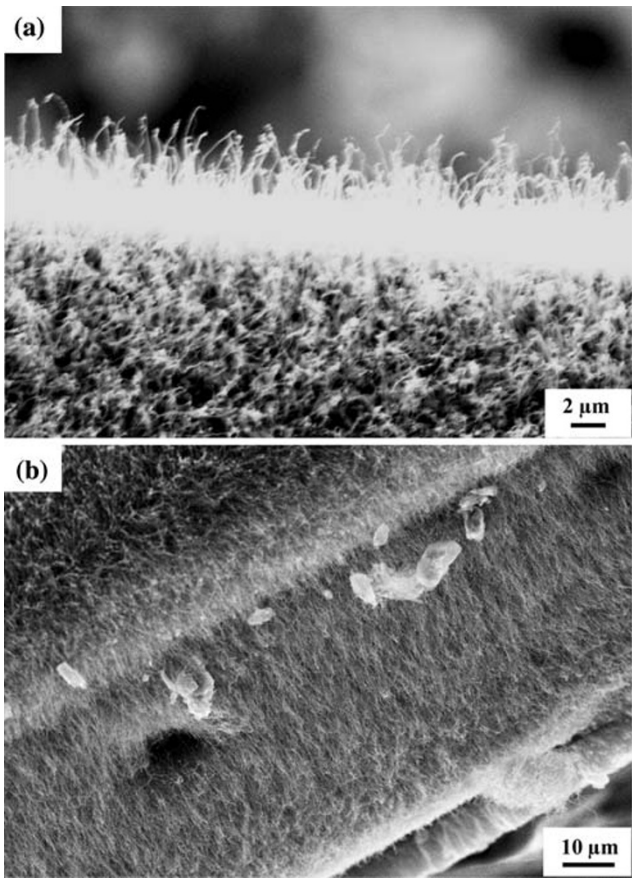

Fig. 3 (**a**) SEM micrograph of a typical CNT film near the edge of the substrate showing CNTs growing outward almost parallel to the substrate: (**a**) top view and (**b**) side view

normal to the lower electrode, i.e., substrate surface facing the microwave source [33]. In our case also, surface plasmon might be generated around the locally existing pores/pits as pit walls are fully or partially normal to the substrate. Therefore, local orientation of field lines around the pits/pores of different size and shapes may be different both in magnitude and direction [34, 35], resulting in flower-like or honeycomb-like morphology of CNTs on the mechanically polished or porous substrates. It is important to note that the effect of electrostatic field is decisive in the initial stage of the growth. However, in the later stage, alignment may be controlled by the crowding effect [10]. The morphology observed in samples 3 and 4 is reproducible with slight variation since it is dependent on the local geometry of the pits/pores. Therefore, if the shape and size of the pits/pores are properly controlled, this process can be used for the synthesis of CNTs with predefined morphology.

Irrespective of the growth morphology of the films, all samples were found to have BS-CNTs. Figure 4a, b shows typical TEM micrographs of BS-CNTs showing base and tip sections, respectively. Each nanotube consists of many short hollow conical compartments stacked in a way such as paper cups. These nanotubes have sharp closed tips and pear/cork-shaped catalytic particles attached at their bases. Some of the BS-CNTs were open in the base region probably because of the detachment of the catalytic particle during specimen preparation. The outer diameter of the BS-CNTs was estimated in the range of 30–70 nm. However, some of the CNTs were of very large diameter ($\sim$150 nm). The tip diameters were in the range of 5–20 nm. The magnified view of a tip section is shown in Fig. 3b. Some of the large diameters BS-CNTs have very irregular and tilted tips. This could be because of the process instability at the nucleation stage of CNTs. These observations clearly suggest that the growth of BS-CNTs in the present study was governed by base mode. High-resolution TEM studies of these CNTs showed many open edges on the outer surface, particularly near the joints of the two compartments [23, 31]. This is accounted to the unique periodic structure (periodic stacking of layers one above the other in such a way to leave uniform outer diameter) of these BS-CNTs. The BS-CNTs were found to be highly crystalline, which has been discussed in detail in our previous articles [30, 31]. The structural characteristics are similar to the nanobells structures called as polymerized carbon nitride nanobells grown by the MPECVD process using methane (CH_4) and nitrogen (N_2) precursors by Ma et al. [26] and Zhang et al. [27]. However, the nanobells did not have regular conical compartments and sharp tip. In addition, the compartments in the nanobells were of much shorter length. The compartments in the present study have more regular conical compartments (Fig. 4a, b).

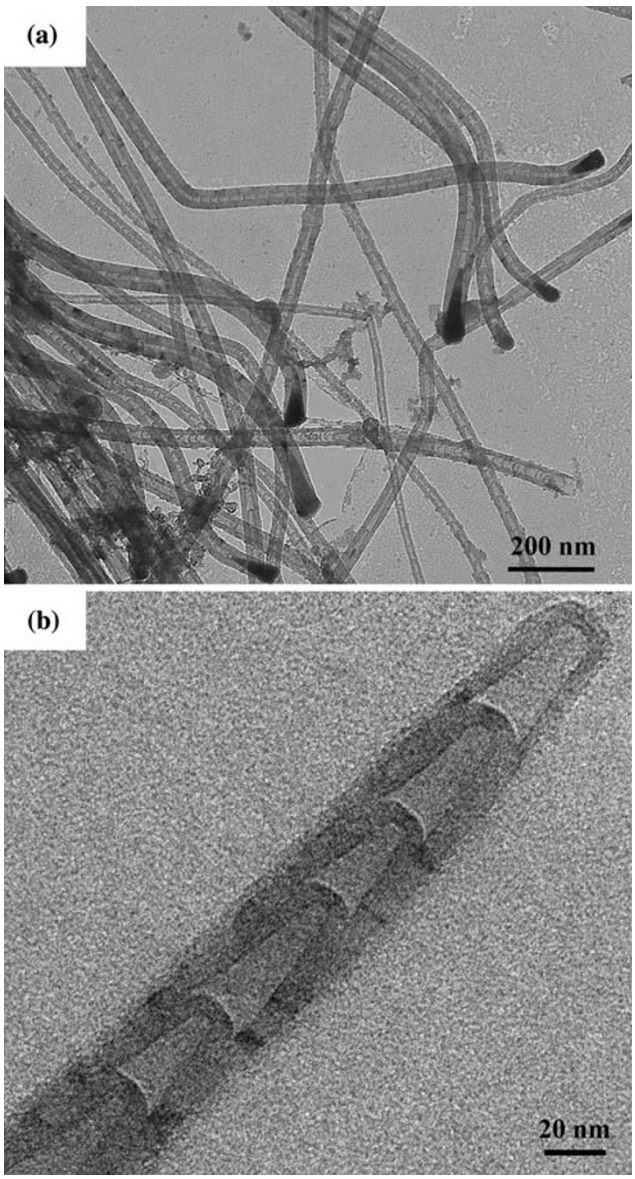

Fig. 4 (**a**) Low magnification representative TEM micrograph of bamboo-structured CNTs, (**b**) magnified view of tip end

EDAX analysis of BS-CNTs was also carried out during TEM investigations (data not shown here) from both with and without metal catalysts regions. The main elements detected were C, O, Fe, Cu, and Si. Cu signal is attributed to the copper micro-grid used for specimen preparation and weak Si signal may be due to the substrate effect. No trace of Al or any other impurities were observed on BS-CNTs surface or in the catalyst particle. However, small amount of nitrogen doping in the BS-CNT films ($\sim$1 at.%) was observed by XPS measurements which get incorporated in BS-CNTs during growth in C_2H_2–NH_3 plasma [31]. Nitrogen plays a critical role in the growth of compartmentalized CNTs or BS-CNTs in plasma CVD process [23, 27]. NH_3 plasma consists of both atomic hydrogen and

nitrogen species compared to only nitrogen species in N_2 gas plasma. Also, it has low dissociation energy compared to N_2 or H_2 and hence is a better dilution gas for the growth of aligned and clean BS-CNTs at a faster rate. In situ optical emission spectroscopy has shown that both hydrogen and nitrogen are essential for the growth of aligned BS-CNTs by MPECVD process, and NH_3 is the main source of atomic hydrogen in C_2H_2–NH_3 composition [23]. Presence of nitrogen in the plasma assures the formation of bamboo-structure causing enhancement in bulk diffusion of carbon in metal (Fe) catalyst. The bulk diffusion is mainly responsible for the compartment formation and hence the bamboo-structure [23]. In addition, nitrogen atoms get incorporated in BS-CNTs, causing change in the electronic structure [27, 30, 31]. Growth mechanism of BS-CNTs and role of nitrogen in the formation of such structures have been discussed in our previous article [23].

Figure 5 shows the comparative plot of integrated emission current density (J) versus applied macroscopic field (E) for four CNT samples. FE parameters such as turn-on (E_{to}) and threshold (E_{th}) fields of these samples are given in Table 1. The E_{th} value observed for four samples is in the range of 2.10–3.55 V/μm. This shows that BS-CNT films have excellent field emission characteristics. The excellent FE characteristics of BS-CNTs films could be attributed to the following: (i) doping of CNTs with N species which may increase the local density of states near

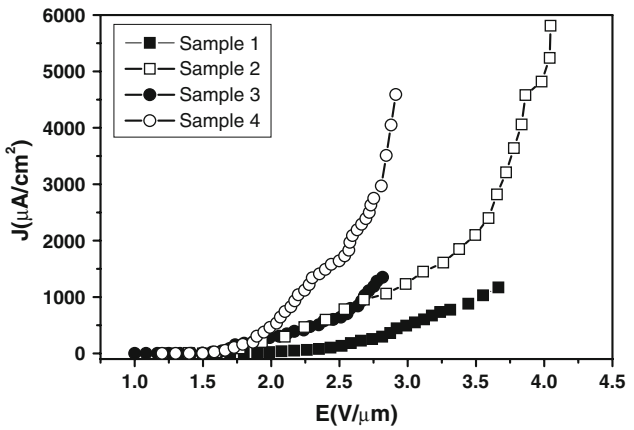

Fig. 5 Comparative emission current density (J) versus macroscopic field (E) plots for CNT samples of different morphology

Table 1 Comparative FE parameters (E_{to}, E_{th}, and β_H) of CNT films grown on different substrate morphology

Sample	E_{to} (V/mm)	E_{th} (V/mm)	Enhancement factor (β_H)
Sample 1	1.95	3.55	6,252
Sample 2	1.40	2.75	12,400
Sample 3	1.50	2.65	12,140
Sample 4	1.55	2.10	9,450

the Fermi level [36–38], (ii) BS-CNTs have lower work function [39] compared to conventional CNTs, (iii) sharp closed tips compared to the lower part of the tube which enhances the aspect ratio, and (iv) metal (catalyst) particles lying at the base of the nanotubes may play important role in improving the emission property providing lower resistance path at the substrate-film interface. The E_{th} value in the present study (2.10 V/μm) is higher than that reported by Ma et al. [26] for polymerized carbon nitride nanobells (1.0 V/μm) synthesized by MPECVD process using N_2 and CH_4 precursors. These nanobells are highly defective. Nitrogen doping reported in their case is $\sim$10 at.% which is very high in comparison to BS-CNT films in the present case ($\sim$1 at.%). High nitrogen doping and hence highly defective structure may be the cause for high emission current at low fields. Also, poor vacuum ($\sim 10^{-6}$ Torr) in the present case compared to Ref. [26] ($\sim 10^{-9}$ Torr) for FE measurements could be another reason for higher E_{th} values.

Among the four samples, sample 4 has shown the best emission characteristics with the lowest E_{th} of 2.10 V/μm while vertically aligned CNT film has the highest E_{th} value. The patterned CNT film (sample 2) also has lower E_{th} value compared to sample 1. The enhanced emission characteristics of BS-CNT films with flower-like or honeycomb morphology are attributed to the existence of many open graphitic edges on the outer surface of the nanotubes along the tube length, particularly near the joints of the two compartments [23]. These open edges on the surface of BS-CNTs act as additional emission sites [30, 31, 40]. On the other hand, in case of vertically aligned BS-CNTs, conventional MWNTs, or single walled CNTs, emission is supposed to occur mainly from the tip section which may further be limited by the screening of the electric field due to neighboring tubes [41]. The screening effect is less effective in case of patterned CNT films. In this case, CNTs in the edge region may dominantly contribute more current than dense interior region. It is to be noted that no significant emission current was observed with porous/mechanically polished Si substrates. This confirmed that emission occurred from CNTs only and not from the edges/protrusions on the substrates. The geometrical enhancement factors (β_H) estimated from slopes of the F–N plots in the high field region were found to be quite high. These are 6,252, 12,400, 12,114, and 9,450 for samples 1, 2, 3, and 4, respectively. Such a high geometrical enhancement factor has been reported in case of open-end CNTs [11].

The sequence of emission patterns of typical BS-CNT films of size $\sim 12 \times 18$ mm^2 grown on porous Si substrates is shown in Fig. 6. The emission patterns were recorded with increasing anode voltage. Initially very few emission sites were found to be active. But the number increased with increase in the applied field and emission from all

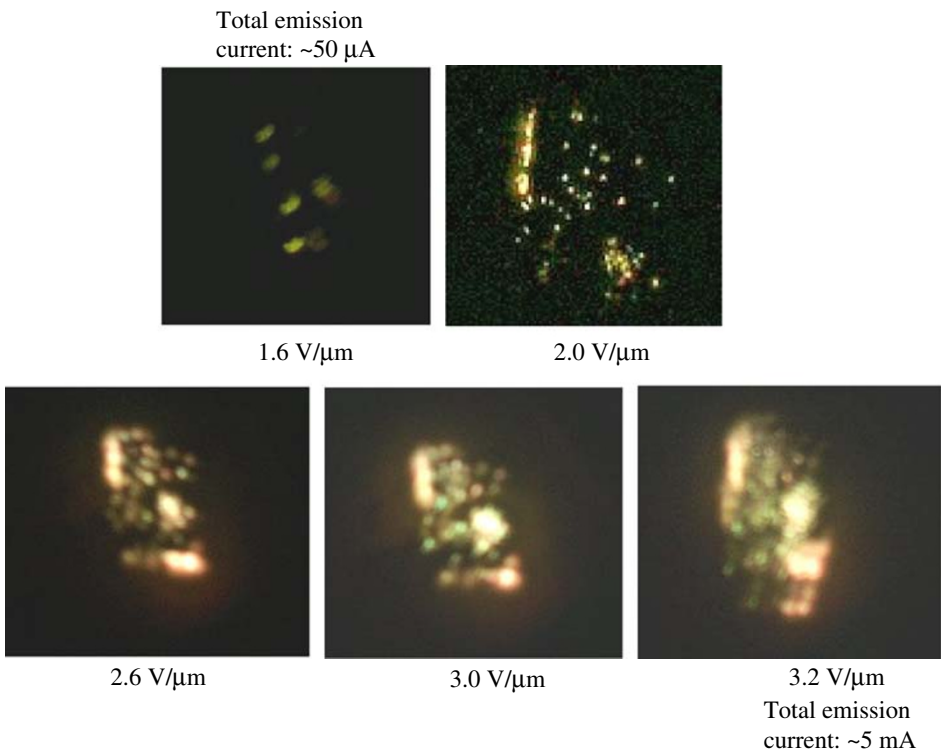

Fig. 6 Sequence of field emission patterns of CNT sample of size $\sim 12 \times 18$ mm^2 on porous Si substrates

parts of the samples was observed above 2.0 V/μm field. However, the emission from all parts of the sample was not uniform. Few regions were found to emit preferably producing high-intensity glow on the anode. This is expected due to the non-uniform surface of sample 4 (Fig. 2d). The non-uniform emission may also be due to the local structure of emitters such as variation in diameter of the BS-CNTs [42]. Low diameter CNTs because of higher aspect ratio may emit preferably at low fields. The comparative FE characteristics of BS-CNTs films with different average diameters from 40 to 165 nm were also investigated. It is found that films with low average diameter nanotubes show the lowest E_{th} value and E_{th} increased with increasing average nanotubes diameter [43].

The multiple color patterns are attributed to the non-uniformity of the CdS film on the TO-coated glass. Initially, light green and blue color spots were seen which slightly turned to yellow and finally orange at higher fields. The color change could also be because of damaging (burning) of the cathodoluminescent Cu:CdS film due to continuous bombardment of the emitted electrons. As a result, the intensity of the some old sites became poor and blurred compared to the fresh ones.

Conclusion

CNT films of different morphology were grown on Si substrates with different initial morphology by MPECVD process. It is found that substrate morphology strongly affects the growth morphology of CNTs in a MPECVD process. Local electrostatic field on the substrate surface in plasma plays a decisive role in growth orientation. However, structural properties of CNTs (bamboo-structure) remained unaffected. It is also found that randomly oriented BS-CNT films are superior emitters compared to that with high-density vertically aligned ones. The defective structure of BS-CNTs and their random orientations have been suggested to be responsible for the enhanced emission characteristics. Emission not only occurs from tips but defects on the body also contribute significantly in randomly oriented BS-CNT films.

Acknowledgments One of the authors (S.K.S.) is very thankful to Mr. Rajesh Pathania, Electron Microscopy Facility, AIIMS, and Dr. D. V. Sridhar Rao, DMRL, Hyderabad, for their support in SEM and TEM measurements, respectively.

References

1. S. Iijima, Nature **354**, 56 (1991). doi:10.1038/354056a0
2. C.A. Spindt, J. Appl. Phys. **39**, 3504 (1968). doi:10.1063/1.1656810
3. P. Gröning, L. Nilsson, P. Ruffieux, R. Clergereaux, O. Gröning, in *Encyclopedia of Nanoscience and Nanotechnology*, vol. 1, ed. by H.S. Nalwa (American Scientific Publishers, 2004), p. 547
4. A.G. Rinzler, J.H. Hafner, P. Nikolaev, L. Lou, S.G. Kim, D. Tomanek et al., Science **269**, 1550 (1995). doi:10.1126/science.269.5230.1550

5. W.A. de Heer, A. Châtelain, D. Ugarte, Science **270**, 1179 (1995). doi:10.1126/science.270.5239.1179
6. P.G. Collins, A. Zettl, Appl. Phys. Lett. **69**, 1969 (1996). doi:10.1063/1.117638
7. Y. Saito, K. Hamaguchi, K. Hata, K. Uchida, Y. Tasaka, F. Ikazaki et al., Nature **389**, 554 (1997). doi:10.1038/39221
8. Q.H. Wang, T.D. Corrigan, J.Y. Dai, R.P.H. Chang, A.R. Krauss, Appl. Phys. Lett. **70**, 3308 (1997). doi:10.1063/1.119146
9. J.M. Bonard, F. Maier, T. Stoeckli, A. Chatelain, W.A. de Heer, J.P. Salvetat et al., Ultramicroscopy **73**, 7 (1998). doi:10.1016/S0304-3991(97)00129-0
10. S. Fan, M.G. Chapline, N.R. Franklin, T.W. Tombler, A.M. Cassell, H. Dai, Science **283**, 512 (1999). doi:10.1126/science.283.5401.512
11. Y. Saito, S. Uemura, Carbon **38**, 169 (2000). doi:10.1016/S0008-6223(99)00139-6
12. J. Yu, Q. Zhang, J. Ahn, S.F. Yoon, Y.J. Li Rusli, B. Gan et al., Diam. Relat. Mater. **10**, 2157 (2001). doi:10.1016/S0925-9635(01)00496-4
13. K.B.K. Teo, M. Chhowalla, G.A.J. Amaratunga, W.I. Milne, G. Pirio, P. Legagneux et al., Appl. Phys. Lett. **80**, 2011 (2002). doi:10.1063/1.1461868
14. S.H. Jo, Y. Tu, Z.P. Huang, D.L. Carnahan, D.Z. Wang, Z.F. Ren, Appl. Phys. Lett. **82**, 3520 (2003). doi:10.1063/1.1576310
15. Y. Chen, Z. Sun, J. Chen, N.S. Xu, B.K. Tay, Diam. Relat. Mater. **15**, 1462 (2006). doi:10.1016/j.diamond.2005.10.063
16. T. Feng, J. Zhang, Q. Li, X. Wang, K. Yu, S. Zou, Physica E (Amsterdam) **36**, 28 (2007)
17. M.P. Siegal, P.A. Miller, P.P. Provencio, D.R. Tallant, Diam. Relat. Mater. **16**, 1793 (2007). doi:10.1016/j.diamond.2007.08.028
18. S.C. Lim, H.J. Jeon, K.H. An, D.J. Bae, Y.H. Lee, Y.M. Shin et al., in *Encyclopedia of Nanoscience and Nanotechnology*, vol. 1, ed. by H.S. Nalwa (American Scientific Publishers, 2004), p. 611.
19. J.-M. Bonard, J.-P. Salvetat, T. Stockli, W.A. de Heer, L. Forro, A. Châtelain, Appl. Phys. Lett. **73**, 918 (1998). doi:10.1063/1.122037
20. W. Zhu, C. Bower, O. Zhou, G. Kochanski, S. Jin, Appl. Phys. Lett. **75**, 873 (1999). doi:10.1063/1.124541
21. D. Zhong, S. Liu, G. Zhang, E.G. Wang, J. Appl. Phys. **89**, 5939 (2001). doi:10.1063/1.1370114
22. J.W. Jang, C.E. Lee, S.C. Lyu, T.J. Lee, C.J. Lee, Appl. Phys. Lett. **84**, 2877 (2004). doi:10.1063/1.1697624
23. S.K. Srivastava, V.D. Vankar, V. Kumar, Thin Solid Films **515**, 1552 (2006). doi:10.1016/j.tsf.2006.05.009
24. H.C. Barshilia, B.R. Mehta, V.D. Vankar, J. Mater. Res. **11**, 1019 (1996). doi:10.1557/JMR.1996.0127
25. S.K. Srivastava, A.K. Shukla, V.D. Vankar, V. Kumar, Thin Solid Films **514**, 124 (2005). doi:10.1016/j.tsf.2005.07.283
26. X.C. Ma, E.G. Wang, Appl. Phys. Lett. **75**, 3105 (1999). doi:10.1063/1.125245
27. G.Y. Zhang, X.C. Ma, D.Y. Zhong, E.G. Wang, J. Appl. Phys. **91**, 9324 (2002). doi:10.1063/1.1476070
28. Z. Xu, X. Bai, Z.L. Wang, E.G. Wang, J. Am. Chem. Soc. **128**, 1052 (2006). doi:10.1021/ja057303j
29. K.B.K. Teo, D.B. Hash, R.G. Lacerda, N.L. Rupesinghe, M.S. Bell, S.H. Dalal et al., Nano Lett. **4**, 921 (2004). doi:10.1021/nl049629g
30. S.K. Srivastava, V.D. Vankar, V. Kumar, Nanoscale Res. Lett. **3**, 25 (2008). doi:10.1007/s11671-007-9109-x
31. S.K. Srivastava, V.D. Vankar, D.V. Sridhar Rao, V. Kumar, Thin Solid Films **515**, 1881 (2006). doi:10.1016/j.tsf.2006.07.024
32. C. Bower, W. Zhu, S. Jin, O. Zhou, Appl. Phys. Lett. **77**, 830 (2000). doi:10.1063/1.1306658
33. Y. Wu, B. Yang, Nano Lett. **4**, 355 (2002). doi:10.1021/nl015693b
34. V.I. Merkulov, A.V. Melechko, M.A. Guillorn, M.L. Simpson, D.H. Lowndes, J.H. Whealton et al., Appl. Phys. Lett. **80**, 4816 (2002)
35. C.C. Lin, I.C. Leu, J.H. Yen, M.H. Hon, Nanotechnology **15**, 176 (2004). doi:10.1088/0957-4484/15/1/034
36. R. Sen, B.C. Satishkumar, A. Govindaraj, K.R. Harikumar, G. Rainja, J.P. Zhang et al., Chem. Phys. Lett. **287**, 671 (1998). doi:10.1016/S0009-2614(98)00220-6
37. L. Qiao, W.T. Zheng, H. Xu, L. Zhang, Q. Jiang, J. Chem. Phys. **126**, 164702 (2007). doi:10.1063/1.2722750
38. Q.B. Wen, L. Qiao, W.T. Zheng, Y. Zeng, C.Q. Qu, S.S. Yu et al., Physica E (Amsterdam) **40**, 890 (2008). doi:10.1016/j.physe.2007.11.015
39. J. Robertson, J. Vac. Sci. Technol. B **17**, 659 (1999). doi:10.1116/1.590613
40. Y. Chen, D.T. Shaw, L. Guo, Appl. Phys. Lett. **76**, 2469 (2000). doi:10.1063/1.126379
41. L. Nilson, O. Groening, C. Emmenegger, O. Kuettel, E. Schaller, L. Schlapbach et al., Appl. Phys. Lett. **76**, 2071 (2000). doi:10.1063/1.126258
42. Z. Xu, X.D. Bai, E.G. Wang, Appl. Phys. Lett. **88**, 133107 (2006). doi:10.1063/1.2188389
43. S.K. Srivastava, V.D. Vankar, V. Kumar, in *Physics of Semiconductor Devices*, 2007. IWPSD 2007 Publication date: 16–20 December 2007, p. 836. Available at http://ieeexplore.ieee.org/xpl